Received: 8 July 2019 | Revised: 27 May 2020 | Accepted: 30 May 2020

DOI: 10.1002/bit.27452

ARTICLE

BIOTECHNOLOGY AND BIOENGINEERING WILEY

Vesicle transport and growth dynamics in *Aspergillus niger*: Microscale modeling of secretory vesicle flow and centerline extraction from confocal fluorescent data

Philipp J. Kunz[1] | **Lars Barthel**[2] | **Vera Meyer**[2] | **Rudibert King**[1]

[1]Chair of Measurement and Control, Technische Universität Berlin, Berlin, Germany

[2]Chair of Applied and Molecular Microbiology, Technische Universität Berlin, Berlin, Germany

Correspondence
Philipp J. Kunz, Chair of Measurement and Control, Technische Universität Berlin, Berlin 10623, Germany.
Email: p.kunz@tu-berlin.de

Funding information
Deutsche Forschungsgemeinschaft, Grant/Award Number: KI 679/10-1 and ME 2041/5-1 within the SPP 1934

Abstract

In this paper, we present a mathematical model to describe filamentous fungal growth based on intracellular secretory vesicles (SVs), which transport cell wall components to the hyphal tip. Vesicular transport inside elongating hyphae is modeled as an advection–diffusion–reaction equation with a moving boundary, transformed into fixed coordinates, and discretized using a high-order weighted essentially nonoscillatory discretization scheme. The model describes the production and the consumption of SVs with kinetic functions. Simulations are subsequently compared against distributions of SVs visualized by enhanced green fluorescent protein in young *Aspergillus niger* hyphae after germination. Intensity profile data are obtained using an algorithm scripted in ImageJ that extracts mean intensity distributions from 3D time-lapse confocal measurement data. Simulated length growth is in good agreement with the experimental data. Our simulations further show that a decrease of effective vesicle transport velocity towards the tip can explain the observed tip accumulation of SVs.

KEYWORDS

Aspergillus niger, filamentous fungi, germ tube, modeling, protein secretion, secretory vesicle

1 | INTRODUCTION

Apart from their enormous ecological importance, filamentous fungi play an outstanding role as biotechnological cell factories of various food ingredients, pharmaceuticals and industrial enzymes (Cairns, Nai, & Meyer, 2018; Meyer, Fiedler, Nitsche, & King, 2015; Punt et al., 2002). One prominent example is *Aspergillus niger*, which has been exploited for the last 100 years as a very efficient multipurpose cell factory for the production of organic acids, proteins, enzymes and drugs.

Filamentous fungal growth takes place solely at the hyphal tips. Hyphae emerge out of swollen spores during a process called germination. Germ tube elongation results in the formation of long hyphae which extend until a certain length, typically around 60–200 µm for *A. niger*, before they start to form septa and multiple branches (Cairns, Zheng, Zheng, Sun, & Meyer, 2019; Cambell, 1971; Trinci, 1974). Ultimately, a hyphal network emerges, which grows radially away from the spore to exploit available nutrient resources. The elongated hyphae contain a system of active transport pathways along cytoskeleton tracks to deliver proteins, lipids and cell wall precursors to the hyphal apex (Steinberg, 2007). This "railway-like" system involves the production of secretory vesicles (SVs), which carry newly synthesized proteins from the endoplasmic reticulum and the Golgi apparatus along microtubules. Microtubules are central elements of the fungal cytoskeleton and, together with motor proteins, are responsible for the long-distance transport of SVs to the hyphal tip, where they typically accumulate. They then become distributed to the actin cytoskeleton, which, in turn, transports SVs to the apical dome, where exocytosis, that is the fusion of SVs with the cell membrane, takes place. As a result, the fungal membrane and cell wall

extend at the tip and proteins are secreted into the surrounding medium (Berepiki, Lichius, & Read, 2011; Lanzetti, 2007; Riquelme, 2013; Steinberg, 2007; Virag & Harris, 2006). The SV fusion with the cell membrane is assumed to be mediated by the soluble NSF attachment protein receptor where NSF stands for N-ethyl-maleimide-sensitive fusion protein (SNAREs; Chen & Scheller, 2001). For this purpose, v-SNARE proteins are included in the vesicle membrane, while the corresponding t-SNAREs are placed into the cell membrane as the target membrane. The SVs in *A. niger* can be tracked using the reporter strain FG7, which expresses an enhanced green fluorescent protein (eGFP) fused with the v-SNARE protein SncA located in the vesicle membrane enclosing the vesicle (eGFP-SncA; Kwon et al., 2014).

Spore germination is a crucial phase in any industrial fermentation. Tip extension highly relies on a coordinated transport to and from the hyphal apex, with SVs as the main tools of cargo delivery. In this study, the temporal change of SV concentration in the early growth phase after germination of *A. niger* is measured by image analysis using the algorithm presented. For interpreting the SV data, we developed a simplistic advection–diffusion–reaction model for SV transport to test whether deceleration of SVs towards the hyphal tip can be used to explain the observed SV accumulation at the tip.

1.1 | Modeling SV transport

Approaches to modeling cargo delivery to the hyphal tip vary immensely in the scale of the specific cell compartments covered. They can be categorized according to the level of detail included, namely as microscale models for phenomena occurring in a single hypha or hyphal tip, mesoscale models describing hyphal network transport and macroscale models for entire fermentation processes (Sugai-Guérios, Balmant, Furigo, Krieger, & Mitchell, 2015). Mechanistic models that couple transport and growth dynamics are typically located in between micro- and mesoscale model types. Only a few studies have specifically simulated production, transport and consumption of SVs inside a single, unbranched hypha.

Prosser and Trinci (1979), as one of the earliest contributions, describe hyphal growth on an agar surface by vesicle production and convective transport to the tip. The spore is described as a simple cell compartment with a SV production term. Branching is considered as a result of vesicle accumulation when the flow is stopped behind the septum. The local resolution is quite coarse, and first-order finite differences are used. Furthermore, the predicted SVs distributions are not confirmed by measured values.

Yang, King, Reichl, and Gilles (1992) calculate tip extension for a filamentous bacterium based on the balance of a limiting key component produced along the length of the hypha and consumed at the tip. The material flow of the key component is treated as being solely due to diffusion. Again, the focus is more on the development of mycelium network structures than on the single hypha. Although the model does well reflect the length growth of the primary branch, it lacks a real, biological counterpart for the key component, which, therefore, was not measured.

López-Isunza, Larralde-Corona, and Viniegra-González (1997) developed a holistic model to simulate convective and diffusive transport of wall precursors and substrate in the cytosol of single *A. niger* hyphae growing on solid medium. They further included substrate diffusion through the solid medium and subsequent uptake following Michaelis–Menten kinetics. Precursor material is formed intracellularly from the substrate and depleted due to the production of cell wall material, that is for elongation. For the simulation of a young germling, the model would have to be extended to include the fungal spore at its boundary. The substrate and precursor concentrations simulated were not verified by measurements; thus, they must be regarded as hypothetical at that point. The SV concentration in the tip region of *A. niger* hyphae is typically increased. Assuming SVs to be the primary tool of cargo delivery, this should, as well, apply for precursor material, but was not replicated in their simulation.

A later model by Balmant et al. (2015) refines their model for single, unbranched aerial hyphae by balancing intracellular maltose concentrations in tank-like compartments along the length of the hypha. They discriminate between a distal nonvesicle-producing zone, a vesicle-producing zone and the transport towards the tip, where vesicles are consumed for tip extension. Production and consumption zones are kept at a constant length, following experimental observations by Trinci (1971). Neither SV nor nutrient concentrations were fit to measured data of *A. niger*. As the model describes the growth of developed aerial hyphae, the tip compartment alone measures at least 10 µm. Thus, the early developmental stages, where the first outgrowth appears and the hyphal tip is yet to be formed, can hardly be described.

Although the longitudinal growth behavior of filamentous fungi has been simulated in the publications mentioned above, none of the studies modeled the early developmental phase of the tip or the formation of the SV tip cluster, which is typical for actively growing hyphae. To fill this gap, our work proposes a basic, extendable mathematical model and compares it to length and SV measurements of an *A. niger* hypha.

This study is structured as follows: First, an image processing algorithm to extract local fluorescence distributions along the centerline of the fungal hypha is described. A quantitative mathematical description of the early germination period in filamentous fungi is then derived and the numerical framework to handle the resulting moving boundary system is presented. Subsequently, exemplary data of the intracellular movement of SVs is processed accordingly and compared against simulation results. Finally, we study the sensitivities of the parameters and initial conditions on length growth and on the SV concentration profiles of the simulation.

2 | MATERIALS AND METHODS

2.1 | Strains and microscopic data acquisition

A. niger spores (1.0×10^5 spores/ml) of strain FG7 (Kwon et al., 2014) were seeded in minimal medium (MM), as described in Meyer, Punt,

and Ram (2010). Cultivation was done in μ-slides VI$^{0.4}$, precoated with poly-L-lysine (ibidi GmbH, catalogue 80604) to ensure spore attachment on the bottom surface of the slide. The inoculated slides were incubated at 37°C, both during 3 hr swelling time and subsequent image acquisition.

The 3D time-series data stacks of germinating spores of *A. niger* were acquired via a confocal laser scanning microscope (CLSM; Leica SP8), utilizing an OPSL laser at $\lambda = 488$ nm for fluorophore excitation and a detector in the range of 490–547 nm to capture emission from eGFP-tagged vesicles (green light emission). Autofocus settings were developed to automatically capture the spores and to stack images equidistantly in a fixed range around them. A laser at $\lambda = 552$ nm wave length, 695–795 nm detector range, was used to avoid extensive photo bleaching during the autofocus procedure, taking advantage of the autofluorescence of the cell wall and avoiding fluorophore excitation. Images were taken with a water immersion objective HC PL APO CS2 63 × /1.20. The voxel depth was set to $d_{\mathrm{Vxl}} = 1.8$ µm, while the pixel width/length was set to $w_{\mathrm{Pxl}} = 0.1$ µm. A lower *z*-resolution was accepted as a compromise between spatial and temporal resolution, while maintaining an acceptable signal-to-noise ratio.

2.2 | Image analysis

The mathematical model ought to be compared against experimental data of the temporal change of relative fluorescent signal intensities of eGFP::SncA in *A. niger*. The data obtained from confocal laser scanning microscopy measurements in this study consists of three-dimensional (3D) image stacks at distinct time points, with one or more fluorescent channels detected. For fitting the model, these data sets are required to be reduced into one dimension by averaging fluorescent image stacks along the discrete medial axis of the hyphae. The challenge of extracting a centerline out of blurry, noise-corrupted confocal image data is interspersed with pitfalls of different kinds. It has been tackled in different segmentation algorithms in the past, most of which originate from medical imaging of human cells, particularly of blood vessels, neurovascular structures or neurites. Referring to the review of Kirbas and Quek (2004), who distinguish between six algorithmic classes, the extraction algorithm developed in this contribution belongs to the first category of classic pattern recognition techniques. It combines elemental filter and segmentation steps in Fiji (Schindelin et al., 2012) with a minimal amount of user interaction necessary.

The CLSM image stacks are preprocessed by background subtraction, denoising by median-filtering and iterative deconvolution. Isotropy is set up by a quadrature interpolation-based reslicing procedure. Furthermore, drift in all spatial directions is compensated for by the realignment plugin "align slices in stack" (Rueden et al., 2017).

Static cultivation without medium flow ensures that the last frame at time t_N captures the centerline positions in all previous frames adequately (i.e. at $t_{1\ldots N-1}$), see Figure 1a. The frame at t_N is first sum-projected into the *xy* plane Figure 1b. It is then binarized, filtered to identify the spore position (Tubeness plugin, ImageJ; Rueden et al., 2017), skeletonized and the projected (*xy*)-centerline $\underline{c}_1(s_1)$ is extracted, Figure 1c:

$$\underline{c}_1(s_1) = \begin{pmatrix} x(s_1) \\ y(s_1) \end{pmatrix}, \tag{1}$$

Note that s_1 is the arc length of the centerline. A list of all abbreviations is given in the supplements. All *z* slices are cut out along the centerline with tubular diameter $w \perp \underline{c}_1$ and straightened along $\underline{c}_1$, using the nonlinear transformation $(x, y, z) \to (\tilde{x}, \tilde{y}, \tilde{z})$ with $\tilde{z} = z$ (FIJI plugin, TransformJ; Meijering, Niessen, & Viergever, 2001). The straightened frame at t_N is sum-projected in the $\tilde{x}$-direction, Figure 1e, and skeletonized to capture the extension in-depth Figure 1f. The resulting skeleton $\underline{c}_2(s_2)$

$$\underline{c}_2(s_2) = \begin{pmatrix} \tilde{y}(s_2) \\ \tilde{z}(s_2) \end{pmatrix} \tag{2}$$

is again transformed according to $(\tilde{x}, \tilde{y}, \tilde{z}) \to (\tilde{\tilde{x}}, \tilde{\tilde{y}}, \tilde{\tilde{z}})$ with $\tilde{\tilde{x}} = \tilde{x}$, Figure 1g. As a result, the hyphal tube is straightened in all spatial directions, with the image dimensions

$$\tilde{\tilde{x}} \in \left[-\frac{w}{2}, \frac{w}{2}\right], \quad \tilde{\tilde{y}} \in [0, L(t)], \quad \tilde{\tilde{z}} \in \left[-\frac{w}{2}, \frac{w}{2}\right]. \tag{3}$$

This final stack is used to extract the intensity profile along $\tilde{\tilde{y}}$, averaging orthogonally in $\tilde{\tilde{x}}$ and $\tilde{\tilde{z}}$, Figure 1h. The steps for skeletonization are displayed in Figure 1i. The one-dimensional mathematical model presented later uses *x* as the spatial coordinate. Therefore, the axial coordinate of a straightened hypha $\tilde{\tilde{y}}$ introduced above will be renamed as *x* in what follows to ease comparison.

The segmentation based on a thresholded projection is not unique, that is, cases can be constructed where either the point of greatest distance from the spore is not the tip but a tight inner curve perpendicular to the view or the longest skeleton branch cannot easily be identified from the projected image (e.g., a star-like structure). The algorithm might, in these cases, fit the centerline to a different centerline, shorter than the longest. Early tip growth after germination, as measured in our experiment, is, however, characterized by rather linear path trajectories, which reduces the risk of the above case occurring.

3 | MODELING

3.1 | Modeling SV tip accumulation

Transport inside a cellular environment can be driven by different mechanisms. Passive diffusion through the cytosol allows molecules to be transferred by thermally driven, random movements but essentially countervails an existing concentration gradient that can be observed in filamentous fungi. Active diffusion, as another mechanism, is caused, for example, by the activity of molecular motors that mix the cytoplasm (Brangwynne, Koenderink, MacKintosh, & Weitz, 2008). By contrast, directed active transport with molecular

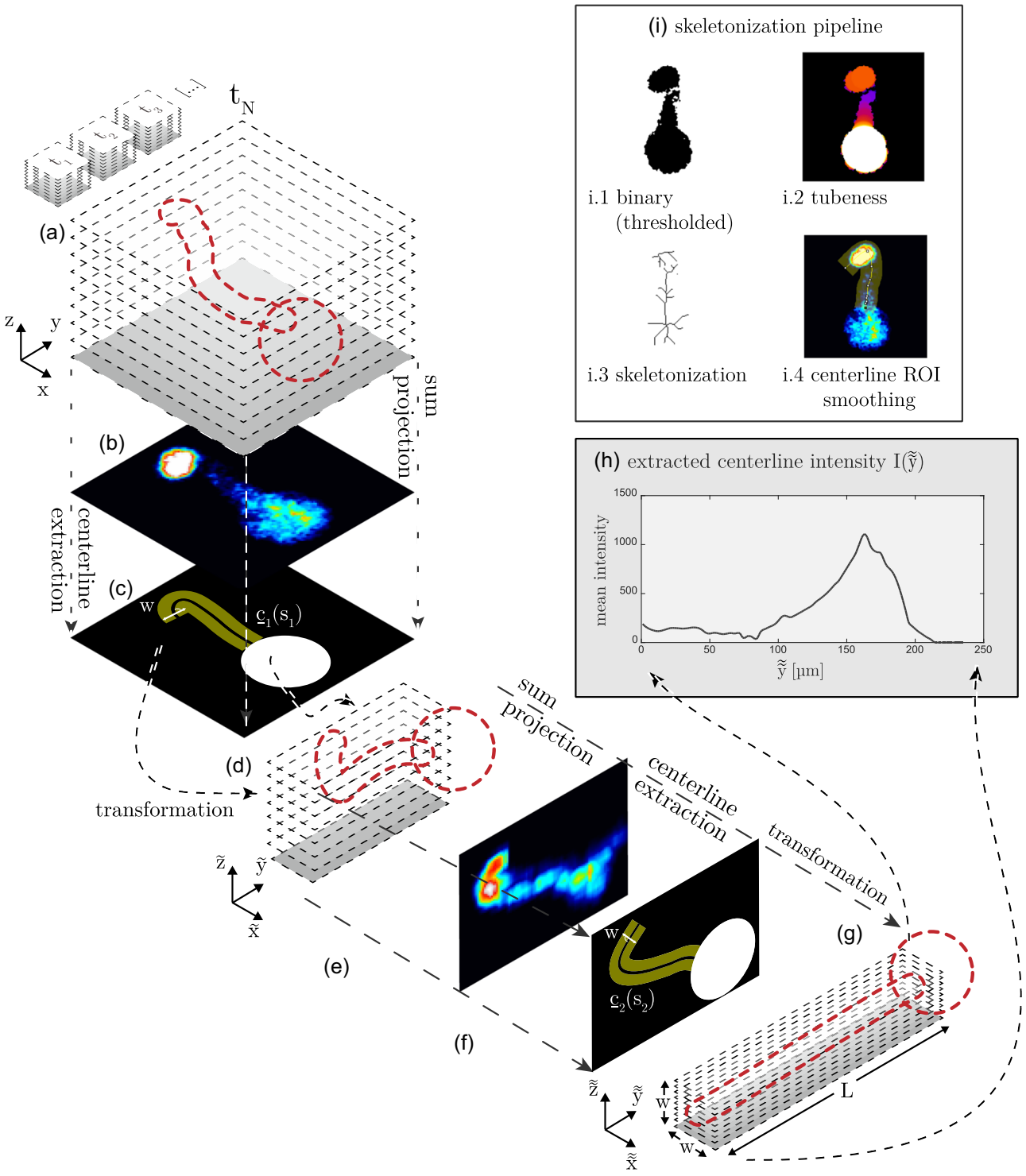

FIGURE 1 Centerline extraction algorithm based on confocal fluorescent image data (measured in CLSM), schematic view: (a) input: stacked time series of single conidium with germ tube, prefiltered, (b) sum projection (*z*-wise) of *N*th time frame, (c) centerline extraction according to skeletonization pipeline (see (h)), (d) straightening along the skeleton in *xy* plane, (e) sum of projection in *w*, (f) centerline extraction, (g) straightening along the skeleton in the $\tilde{y}\tilde{z}$ plane, (h) extraction of mean intensities on $\tilde{\tilde{x}}\tilde{\tilde{z}}$ planes orthogonal to $\tilde{\tilde{y}}$ results in mean centerline intensity as a function of the hyphal length, and (i) skeletonization pipeline: thresholding, radius estimation with tubeness ImageJ plug-in (Rueden et al., 2017), skeletonization and centerline extraction [Color figure can be viewed at wileyonlinelibrary.com]

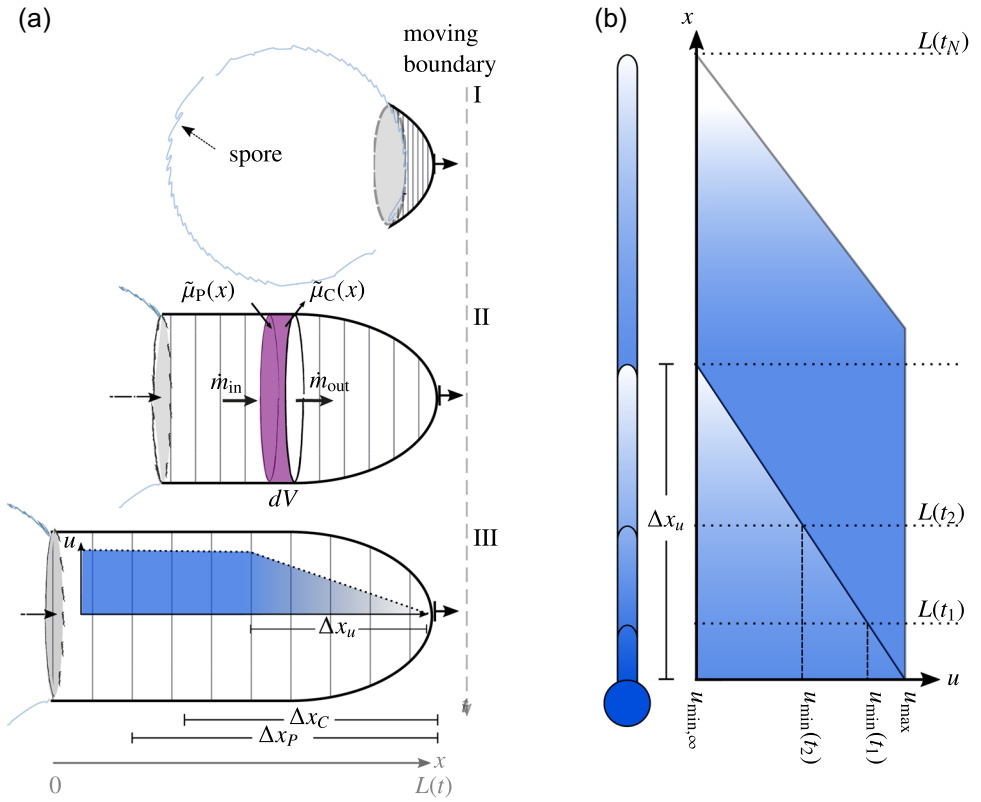

FIGURE 2 (a) Algorithmic details during the stretch phase. I: Young hyphal tip after germination, right tip boundary moves away; II: while the grid is stretched equidistantly, secretory vesicle fluxes, local production, and consumption are balanced inside a volume element dV; III: developed consumption zone Δx_C and deceleration zone Δx_u stay stationary relative to the hyphal tip. (b) Development of the tip velocity gradient during outgrowth: Velocity at the spore surface is held constant, while velocity at the tip $u_{min}(t)$ decreases to a minimum until condition $L(t) = \Delta x_u$ is met. Subsequently, the deceleration zone moves in parallel to the tip [Color figure can be viewed at wileyonlinelibrary.com]

motor proteins (such as the kinesins), along microtubules allows the cell to transfer cargo at the cost of adenosine triphosphate (ATP). Furthermore, an unbound molecule can be transported passively inside the intracellular stream of the cytoplasm. In *A. niger*, active transport is the determining mechanism behind the long-distance transport and accumulation of SVs (Steinberg, 2007).

Individual SVs move at a pace above the velocity of hyphal extension. Near the tip, their concentration is not constant but shows a gradient along the length of the hypha, as apparent in microscopic images (see Figure 3a). We will, hereafter, assume that the transport speed on subapical microtubules exceeds the velocity expected on apical actin cables, that is the velocity reduces towards the tip. Cross-linking between both structures is very likely (Elie et al., 2015). Thus, the transition between both velocities will be rather smooth. In this article, we investigate whether a linear decrease in transport velocity towards the hyphal tip can be used to explain the formation of the observed SV tip accumulation.

3.1.1 | Model assumptions

Our dynamic model describes the active transport of SVs along microtubules (MT) inside the hyphal tube as well as diffusive vesicle motion at its tip. During the time period covered by the model, neither septation nor branch initiation has taken place and intracellular vesicle flow is neither stopped nor decreased elsewhere than in the tip region. Substrate uptake or secretion are not considered explicitly but can be included in the model structure. Furthermore, we do not distinguish between microvesicles and macrovesicles, which carry different kinds of enzymes, synthesizing the cell wall (Riquelme, 2013). Hence, all vesicles are assumed to be fully loaded (or at a constant ratio). Recycling of SVs after cargo release is not integrated into the model.

SVs will hereafter be represented as continuous, local concentrations $\mathcal{V}(x)$ as the product of the local microtubule density ($\frac{m_{MT}}{V}$) and the vesicles per microtubule ($\frac{m_{\mathcal{V}}}{m_{MT}}$). A local mass of substance i is denoted by m_i, and dV represents the local volume. Although it seems to be a rather rough approximation of the discrete nature of cellular vesicles, it is considered an appropriate simplification (see Diehl, Henningsson, Heyden, & Perna, 2014). Morphologically, the main part of hypha can be described as a cylinder with a constant diameter, which decreases locally at the hyphal tip. The tip radius is not considered a necessary element in the simulation for two reasons: First, from experimental images, see Figure 3a, the quasi-stationary SV buffer region spans a much wider zone behind the apex than just the region of diameter decrease. Secondly, SV

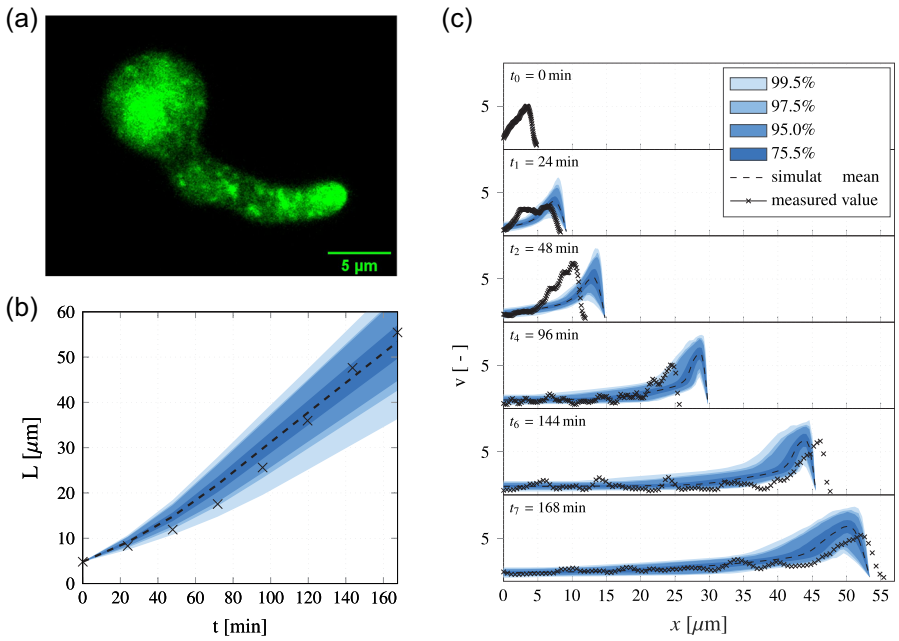

FIGURE 3 (a) Germ tube after germination from the spore (left). Z-projected time frame from the confocal stack. Green fluorescence from marker strain indicates vesicle accumulation in the spore and at the tip. (b) Germ tube length growth over time. (c) Secretory vesicle concentration profiles of an example germling at successive time steps. *left boundary*: spore and *right boundary:* hyphal tip. A steady accumulation develops behind the tip. Data obtained from confocal images using the centerline extraction algorithm (Figure 1). Time frames from t_0 = 0 to t_7 = 165 min after spore germination [Color figure can be viewed at wileyonlinelibrary.com]

transport velocity at the very tip is assumed to be close to 0. Therefore, a decrease in diameter would not show strong effects on the simulation. The radius is, thus, held constant mathematically at a mean measured radius of $r = 3.73/2$ µm.

3.1.2 | Balancing equations

Starting with a general mass balance for the infinitesimal small volume dV,

$$\frac{\partial m_{\mathcal{V}}(x,t)}{\partial t} = \dot{m}_{\mathcal{V}}(x,t) - \dot{m}_{\mathcal{V}}(x+dx,t) + (\mu_P(x,t) - \mu_C(x,t))dV \tag{4}$$

results, with a vesicle mass flow $\dot{m}_{\mathcal{V}}$ entering the balance volume dV at x and leaving it at $x + dx$. Volumetric vesicle production and consumption terms are given by $\mu_P(x,t)$ and $\mu_C(x,t)$, respectively (see Figure 2a, II). Since SVs are produced inside the organism and cannot cross cell wall boundaries, there is no transport from or to the environment.

The mass flow of vesicles $\dot{m}_{\mathcal{V}}$ can be replaced by a flux density term in the x-direction, j_x, or more refined by the vesicle concentration $\mathcal{V}(x,t)$ by combining the advective transport with velocity $u(x,t)$ due to active movement and the diffusion of unbound vesicles:

$$\dot{m}_{\mathcal{V}}(x,t) = j_x A = \left(\mathcal{V}(x,t)u(x,t) - D\frac{\partial \mathcal{V}(x,t)}{\partial x}\right)\cdot A. \tag{5}$$

Hence

$$\frac{\partial m_{\mathcal{V}}(x,t)}{\partial t} = [j_x(x,t) - j_x(x+dx,t)]\cdot A + (\mu_P(x,t) - \mu_C(x,t))\cdot dV. \tag{6}$$

Expansion of the second term on the right-hand side of Equation (6) into a Taylor series gives

$$j_x(x+dx,t) \approx j_x(x,t) + \frac{\partial j_x(x,t)}{\partial x}dx, \tag{7}$$

while neglecting all terms in $(dx)^n$, $n \geq 2$ leads to

$$\frac{\partial m_{\mathcal{V}}(x,t)}{\partial t} = -\frac{\partial j_x(x,t)}{\partial x}Adx + (\mu_P(x,t) - \mu_C(x,t))\cdot dV. \tag{8}$$

Inserting $m_{\mathcal{V}}(x,t) = \mathcal{V}(x,t)\cdot dV$, differentiating with respect to t and dividing by $dV = A\cdot dx$, yields

$$\frac{\partial \mathcal{V}(x,t)}{\partial t} = \underbrace{-\frac{\partial}{\partial x}\left(\mathcal{V}(x,t)u(x,t) - D\frac{\partial \mathcal{V}(x,t)}{\partial x}\right)}_{\text{I}} + \underbrace{(\mu_P(x,t) - \mu_C(x,t))}_{\text{II}}. \tag{9}$$

The first term on the right-hand side describes the change of concentration due to internal fluxes, while the second captures source and sink terms due to vesicle production and consumption,

respectively. $u(x,t)$ represents a mean value, that is the active transport velocity on microtubules per local hyphal area A, while D, as the diffusion constant, quantifies random movements of unbound vesicles in the tip area. Equation (9) is normalized by a normalization concentration $\mathcal{V}_0$ with $v(x,t) = \frac{\mathcal{V}(x,t)}{\mathcal{V}_0}$ and $\mu'_i(x,t) = \frac{\mu_i(x,t)}{\mathcal{V}_0}$ to allow for a parameter fit to different extracted centerline profiles, yielding

$$\frac{\partial v(x,t)}{\partial t} = -\frac{\partial}{\partial x}\left(v(x,t)u(x,t) - D\frac{\partial v(x,t)}{\partial x}\right) + (\mu'_P(x,t) - \mu'_C(x,t)). \tag{10}$$

3.1.3 | Moving boundary problem

New balance volume is formed while the tip grows out of the spore (Figure 2a), but existing SVs are already present inside the germ tube. The problem is treated like a moving boundary problem to solve the transport equation on the growing balance domain (while keeping a confined number of numerical grid points and, therefore, equations to solve after subsequent discretization). Hence, the mathematical system is transformed according to Crank's front-fixing method (Crank, 1987), which artificially fixes the grid on the dimensionless axial coordinate $\eta = \frac{x(t)}{L(t)} \in [0,1]$ with the moving boundary at $\eta = 1$. The relationship $f(x,t) = \tilde{f}(\eta,t)$ must be maintained for $x = L\eta$ for an arbitrary function in the x-coordinate $f(x,t)$ to be transformed into $\tilde{f}(\eta,t)$. The basic model equation (9) is transformed accordingly into fixed coordinates (see the full derivation in Appendix B):

$$\frac{\partial \tilde{v}(\eta,t)}{\partial t} = -\frac{\partial}{\partial \eta}\left(\tilde{v}(\eta,t)u(\eta,t) - \frac{D}{L(t)}\frac{\partial \tilde{v}(\eta,t)}{\partial \eta}\right)\frac{1}{L(t)} + (\tilde{\mu}'_P(\eta,t) - \tilde{\mu}'_C(\eta,t)) + \frac{\partial \tilde{v}(\eta,t)}{\partial \eta}\left(\frac{\eta \dot{L}(t)}{L(t)}\right). \tag{11}$$

Consequently, the total number of grid points N in the numerical grid stays constant when the hyphal tip extends. The transformative rule is, therefore, equivalent to an equidistant stretching of the numerical grid, while inserting an artificial flux term to cope with the increase in length. For simplicity, all following expressions concerning kinetics and boundary/initial conditions will be given as functions of the x-coordinate, but solved in this numerical scheme as functions of η.

3.1.4 | Initial and boundary conditions

The system is well-posed only if proper boundary and initial conditions are defined. As swelling conidia show considerable secretory vesicle activity, it can be reasonably assumed that vesicle flux from the spore contributes to tip growth in the very first period after germination. Since the vesicle flow from the spore into the germ tube is unknown and its contribution to tip growth decreases with increasing hyphal length, imposing a specific mass flux at the left boundary does not seem a sensible solution. Instead, we can set the boundary concentration $v(0,t) = 1$ directly if we normalize the measured intensity profiles by the stationary left boundary value at later time steps, that is when the tip body has fully developed. However, when the germ tube is still short, the left boundary value is enhanced by the evolving vesicle cluster, which is depleted when the tip moves forward after germination. As a first approach, we assume that the left boundary converges to $v(0,t) = 1$ according to a simple model

$$\dot{v}(0,t) = 1 - v(0,t). \tag{12}$$

At the end of the germ tube, SVs are either fused with the cell membrane or recycled internally. Therefore, the right boundary is assumed to be perfectly absorbing, and the concentration is fixed at $v_{x=L} = 0$. The first measured hyphal length value and concentration profile are taken as initial length and initial distribution, respectively.

3.1.5 | Kinetics

For Equation (11), expressions for consumption, tip growth, production, transport and diffusion have to be specified.

Consumption

We assume that the hyphal extension rate links to the vesicle fusion at the tip membrane, that is faster growth necessitates higher tip consumption of SVs. The consumption term $\tilde{\mu}'_C(x,t)$ describes this mechanism. Consumption by cell membrane fusion is further assumed to be restricted to a consumption zone Δx_C behind the apex where vesicles merge with the extending cell membrane (Figure 2a). It exhibits saturation kinetics because a carrier complex mediates SV fusion:

$$\tilde{\mu}'_C(x) = \begin{cases} \frac{k_C \cdot v(x)}{K_C + v(x)} \frac{1}{A(x)\Delta x} & \text{if } L(t) - \Delta x_C \le x \le L(t), \\ \text{otherwise } 0, \end{cases} \tag{13}$$

where K_C is the empirical saturation constant and k_C is the maximal elongation velocity. We calculated $\Delta_C = 13\,\mu m$ by scaling the zone length obtained in Balmant et al. (2015) to the diameter of *A. niger*.

Tip growth

Elongation of the first hypha after germination typically undergoes a transition from exponential to linear length growth dynamics (Fiddy & Trinci, 1976; Gougouli & Koutsoumanis, 2013; King, 2015; Nanguy, Perrier-Cornet, Bensoussan, & Dantigny, 2010) and is modeled by a Monod-type kinetic expression, as a function of the sum of consumed SV in all grid cells within the consumption zone Δx_C. Furthermore, we add the flow of SVs that pass from the penultimate (i.e., the $N-1$th) node to the absorbing right boundary:

$$\frac{dL}{dt} = Y_L\left(\sum_{i=N-N_c}^{N} (\tilde{\mu}'_C(x_i)V_i) + v_{N-1}u_{N-1}A_{N-1}\right), \tag{14}$$

where Y_L is the extension of hyphal length per (dimensionless) mass of vesicle consumed.

Production

We expect vesicle synthesis to take place in the last Δx_P behind the tip of the young germ tube. Out of a general range of 5 $\mu m \leq \Delta_P \leq 20$ μm for filamentous fungi, as stated by Sugai-Guérios et al. (2015), we choose the maximum $\Delta_P = 20$ µm as an estimate. As a first attempt, we propose a fixed production rate, θ_P, following Steinberg and Schuster (2011), who observed a relatively homogeneous distribution of Golgi equivalents (and, therefore, SV sources) in the tip area of *A. nidulans*:

$$\tilde{\mu}'_P(x) = \begin{cases} \theta_P & \text{if } L(t) - \Delta x_P \leq x \leq L(t) \quad \text{and} \quad v(x) > 0, \\ \text{otherwise} \quad 0, \end{cases} \tag{15}$$

Transport

As a first approach, transport speed is set to be at a constant value u_{max} within the subapical hypha and to decrease linearly from this value to $u_{min}(t)$ at the very apex within the deceleration region Δx_u:

$$u(t,x) = \begin{cases} u_{max}, & \text{if } x \leq L(t) - \Delta x_u, \\ u_{max} - \dfrac{u_{max} - u_{min}(t)}{\Delta x_u}\Big(x - L(t) + \Delta x_u\Big), & \text{if } x > L(t) - \Delta x_u. \end{cases} \tag{16}$$

During the early growth phase after germination, when Δx_u is not yet established, $u_{min}(t)$ decreases over time, until the condition $L(t) = \Delta x_u$ is met:

$$u_{min}(t) = u_{max} - \frac{u_{max} - u_{min,\infty}}{\Delta x_u} \cdot L(t). \tag{17}$$

$u_{min,\infty}$ is set to zero so that SVs decelerate until the velocity of the moving apex. Figure 2b visualizes the time-dependent velocity profile. It should be mentioned that the course of the decrease in speed and how the velocity gradient builds up dynamically is largely unknown. Notably, an abrupt transition between MT and actin velocities would lead to a rapid accumulation in the first actin element in the simulation, which was deemed unlikely. Moreover, numerical issues due to the step in concentration are avoided by assuming a gradual reduction of the velocity.

Diffusion

If SVs were considered completely unbound and free to move inside the cytoplasm, the Einstein-Smoluchowski relationship would probably hold (Einstein, 1926/1956). However, studies revealed that vesicle-sized particles move significantly more slowly in the cytosolic environment (Luby-Phelps, 1999). Furthermore, as current scientific findings suggest an actin-mediated, star-shaped transport pattern in the apical dome, effective diffusion will merely serve as a simplified way to model isotropic cargo redistribution with the diffusion constant $D = 5\ \mu m^2 \cdot min^{-1}$. Diffusion is expected in the whole compartment behind the spore, due to the lack of septation in the young germ tube (Trinci, 1974).

3.2 | Parameter identification procedure

The model parameters were identified by fitting the model to the measured SVs profiles and the length growth of the hypha. To ensure a priori identifiability of the model, some parameters were fixed either by approximate calibration or from literature data. This was necessary because several parameters (like k_C and Y_L) were mathematically dependent. The parameters $\underline{\theta}^T = (k_C, \Delta x_u, \theta_P)$ were altered for fitting the model. Table 1 lists all parameters that were fixed and estimated during the procedure. A combination of methods, both global and local, was used for the parameter identification: Starting with a global search, a multistart optimizer routine drew starting values as Latin hypercube samples from the parameter space. Further, simulated annealing (Matlab, Opt. toolbox) followed to assure the global minimum was found. Locally, TOMLAB SNOPT 6.7 and downhill simplex (Press, 2002) were used to improve the estimate

TABLE 1 Best-fit parameter estimates and values of fixed parameters

Parameters		Estimate	±σ MCMC	Unit
$\hat{k}_C$	Max. specific growth rate	3.13	1.91 (61.0%)	min^{-1}
$\hat{\Delta x}_u$	Width of velocity gradient	4.85	0.27 (5.6%)	µm
$\hat{\theta}_P$	Production factor	1.10	0.14 (12.7%)	$Ves \cdot \mu m^{-3} \cdot min^{-1}$
Fixed parameters		**Value**	**Unit**	**Source/estimate**
K_C	Half velocity constant	200	$Ves \cdot \mu m^{-3}$	Estimate
r	Hyphal radius	3.726/2	µm	Measured
u_{max}	Max. advection velocity	10.0	$\mu m \cdot min^{-1}$	Schunck, Herrero, & Fischer (2011)
D	Diffusion constant	5.00	$\mu m^2 \cdot min^{-1}$	Estimate
Δx_P	Width of production zone	20.00	µm	Sugai-Guérios et al. (2015)
Δx_C	Width of consumption zone	13.00	µm	Balmant et al. (2015)
Y_L	Extension factor length growth	2×10^{-2}	$\mu m \cdot Ves^{-1}$	Fixed

further. Parameter confidence intervals were computed using a Bayesian importance sampling approach (MCMC, viz., parallel tempering, using the PESTO toolkit by Stapor et al., 2018). As an objective function for parameter estimation, a combination of an unweighted least-squares formulation for vesicle concentration and length was calculated

$$\chi^2(\underline{\theta}) = \sum_{i=1}^{N_t} (\underline{y}^M(t_i, \underline{\eta}) - \underline{y}(t_i, \underline{\eta}, \underline{\theta}))^2 + \sum_{i=1}^{N_t} (L^M(t_i) - L(t_i, \underline{\theta}))^2. \tag{18}$$

Here, the superscript M indicates measured values, that is $\underline{y}^M$ and L_k^M are measurements obtained from the centerline extraction. $\underline{y}$ and L are the simulated prediction of vesicle concentration and hyphal length, respectively. For normally and identically distributed measurement noise, minimizing $\chi^2(\underline{\theta})$ corresponds to a maximum likelihood estimation and χ^2 is minimal for $\underline{\theta} = \hat{\underline{\theta}}$.

The samples from the converged MCMC chains were used to (a) calculate the parameter uncertainties and (b) were propagated through the model to obtain predictive uncertainty bounds. The parameter uncertainties, as calculated from the MCMC chains, σ_{MCMC}, indicate how strongly these parameters influence the objective function. For obtaining the prediction bounds (marked as blue areas in Figure 3b,c) we forwarded the sampled MCMC parameter sets through the model to receive a set of simulation trajectories. From these simulations, we could draw population statistics, that is the mean and the levels of confidence (as $100\%[1-\alpha]$ with $\alpha = [0.005, 0.025, 0.05, 0.25]$) calculated per time or per grid point.

3.2.1 | Model implementation details

The partial differential equation (11) is solved using the method of lines, that is by the discretization and calculation of spatial derivatives with finite difference stencils. As tip-accumulated vesicles typically show sharp gradients, standard linear finite difference stencils (such as upwind or central) will result in numerical artifacts and cannot be used. Therefore, high-order spatial derivatives are calculated using polynomial reconstruction with pre-computed weights, rooting to the work of Shu (1998). The resulting system of ODEs is solved using an explicit Runge–Kutta routine in *C*, which was compiled and executed in MATLAB. We used an Intel Core i7-6700 3.40 GHz CPU, 32 GB RAM system for all calculations involved in this study.

4 | RESULTS

Model parameters were fit to a germ tube that was representative of the population. The predicted length growth (simulated mean) of *A. niger* is compared to measured values in Figure 3b. Uncertainty bounds for the simulation are plotted in shades of blue, based on the empirical quantiles of the predicted length growth and vesicle distributions outlined above. Simulative and measured length data points match closely. Length is overestimated slightly at times $t < 120$ min; however, all measured values lie within predicted uncertainty bounds at all times. This overestimation carries over to the comparison of measured and simulated SV evolution that shows an excellent fit of the space-dependent concentration profile, but lacks the correct length. Figure 3c shows both the simulated SV profiles and the measured SV data for the extension of an *A. niger* hypha at different times. The left and right boundary mark the position of the spore and the hyphal tip, respectively. The SV concentration increases towards the tip then decreases quickly at the apex due to SV consumption. Since SVs are only produced in the last 20 µm behind the tip, and the left boundary value rapidly converges to 1, normalized concentration in the subapical part is 1. The simulated SV profiles are consistent with the measured data as a steady tip gradient is developed and progresses over time. During the establishment of the tip accumulation at times $t < 50$ min, the model prediction falls below the measured concentration, as the concentration gradient cannot be built up quickly enough.

The parameter estimates $\hat{\underline{\theta}}$ obtained from the identification procedure are shown in Table 1. The estimated length of the velocity deceleration zone $\hat{\Delta}x_u$ spans the last 4.85 µm of the germ tube. The estimated production factor is $\hat{\theta}_P = 1.10\,\text{Ves}\cdot\mu\text{m}^{-3}\,\text{min}^{-1}$. The estimate for the maximum specific growth rate shows high uncertainty with a relative error of 61.0%. The MCMC results (Appendix C) prove a negative correlation between the production factor $\hat{\theta}_P$ and $\hat{k}_C$: When more SVs are produced, fewer SVs are consumed in order not to exceed elongation velocity.

4.1 | Sensitivity analysis

A sensitivity analysis was conducted to determine to what extent the model parameters and the initial conditions influence the length and the SV distribution of an *A. niger* hypha. For comparison, the reference time $t = 150$ min was chosen. Relative length deviation is plotted against parameter variation in Figure 4a. The effect of the parameters on SV profiles is plotted in Figure 4b. Y_L shows a strong impact on the hyphal length, as the parameter directly determines the length increase per SVs consumed. The SV velocity v_{ves} has a greater influence because the material is delivered to the tip more quickly with increasing SV velocity. The effects of the parameters k_c and K_c on hyphal length at $t = 150$ min are insignificant. The sensitivities of length growth on D and Δx_u are almost identical, but their influences on vesicle accumulation are very different: When increasing diffusion (increasing D), less vesicle material reaches the tip and the vesicle cluster is flattened. When SVs decelerate over a wider region (increased Δx_u), more vesicles are held back and the tip cluster is amplified. At the same time, fewer SVs attain the right boundary where they could contribute directly to tip elongation.

The initial SV profile was multiplied by a factor f_{IC} to test the influence of varying initial conditions, as plotted in Figure 4a. The length deviation scales linearly, since more SVs linearly translate into

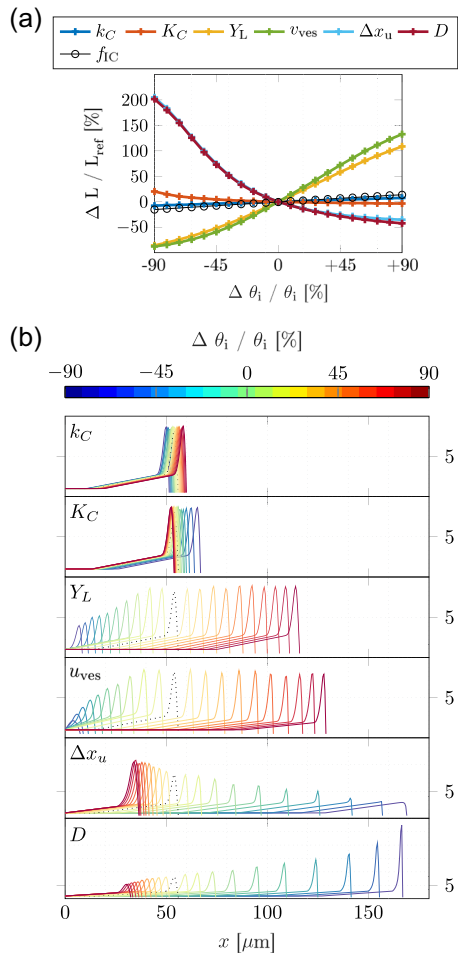

FIGURE 4 (a) Relative length change with varying parameter values at t = 150 min. (b) Sensitivity analysis of the best-fit parameters and the initial conditions on simulated hyphal length and SV concentration profiles [Color figure can be viewed at wileyonlinelibrary.com]

length growth, following Equation (14). The effect of f_{IC} on hyphal length, however, is low compared to the effects of the model parameters.

5 | DISCUSSION

In this article, we derived a model to describe the build-up of the SV tip cluster in young *A. niger* hyphae after germination. The model was fit to intracellular SV concentration measurements, which were obtained from 3D confocal laser scanning microscopy data by using the centerline algorithm described. This processing algorithm developed extracts mean axial distributions from 3D time-lapse data of hyphal objects and was used to quantify SVs inside young *A. niger* hyphae. The algorithm could be used to quantify the density of other cell organelles from fluorescent confocal image stacks and will set the data basis for future transport modeling approaches. However, the algorithm places relatively high demands on the position of the sample objects (in this case: of the individual spores and the hyphae), as they need to be clearly separated from each other in the image. In this experiment, the germinating spores formed relatively few clusters, which was due to the low spore density.

The mathematical model describes fungal tip extension and transport of SVs in young *A. niger* hyphae, which develop from spores or as new branches in growing mycelia. The model uses a fixed rate to describe SV production and saturation kinetics to model SV consumption due to fusion with the cell membrane. Both SV production and consumption terms are restricted to distinct zones behind the apex, which ensures that individual hyphal tips can grow independently and on self-supply. The growth equation in the model is a function of the mass of vesicles fusing with the cell membrane. As a first step, we wanted to test the hypothesis that a simple decrease in transport velocity towards the apex could be responsible for the increased SV occurrence in the apical dome. With the overall model, the key phenomenon of SV accumulation at the hyphal apex, as well as the speed of tip extension, could be replicated. The model showed weaknesses in the description of the early formation of the tip profile, see Figure 3c.

A mathematically similar approach has been used to model the growth of fungal aerial hyphae (Balmant et al., 2015). Although the model has not been validated for *A. niger* and its tank-like discretization is too coarse for hyphae in such early stages of development, it would be interesting to compare its abilities to describe SV accumulation in fully grown hyphae.

The parameter estimation result proved the overall ability of the model to describe the dynamics of the establishment of high vesicle density at the tips of young germ tubes in *A. niger*. Our assumption that the effective transport velocity decreases towards the tip led to transport dynamics in good agreement with the SV measurement data. An extended number of young germ tubes would have to be taken into account to quantify the apparent growth and transport heterogeneity among outgrowing hyphae in future studies. Notably, uncalibrated confocal microscopy can only provide relative values of the vesicle concentration, which depend on multiple experimental factors. On the one hand, this allowed us to normalize the image data. On the other, the kinetic parameters identified under these conditions are also normalized values and, therefore, lack the ability to predict absolute vesicle densities. In situ measurements of the absolute SV concentrations in the cytosol could deal with these restrictions. It will serve to quantify variation in SV distribution between static and flow cultivation conditions to address the question of SV involvement in cell-wall stabilization.

This basic model structure generally allows quick testing of transport hypotheses inside unbranched filamentous fungi. Secretion dynamics can be included in the model structure at any time and can be compared to appropriate measurements. To extend the model approach to the description of complex mycelia, each branch in the mycelium would have to be modeled by a set of discretized equations to be solved simultaneously. Branches at which the flow is divided into several side branches must be taken into account in the boundary conditions. Special attention should be paid to an efficient

strategy when choosing the solver. All these issues will be dealt with in future studies.

ACKNOWLEDGMENTS

The authors thank the Deutsche Forschungsgemeinschaft (DFG) for the financial support for this study (KI 679/10-1 and ME 2041/5-1) within the SPP 1934 DiSPBiotech.

ORCID

Philipp J. Kunz http://orcid.org/0000-0001-6533-7438
Lars Barthel https://orcid.org/0000-0001-8951-5614
Vera Meyer https://orcid.org/0000-0002-2298-2258
Rudibert King https://orcid.org/0000-0002-0997-0498

REFERENCES

Balmant, W., Sugai-Guérios, M. H., Coradin, J. H., Krieger, N., Furigo Junior, A., & Mitchell, D. A. (2015). A model for growth of a single fungal hypha based on well-mixed tanks in series: Simulation of nutrient and vesicle transport in aerial reproductive hyphae. *PLOS One*, *10*, 1–22. https://doi.org/10.1371/journal.pone.0120307

Berepiki, A., Lichius, A., & Read, N. D. (2011). Actin organization and dynamics in filamentous fungi. *Nature Reviews Microbiology*, *9*, 876–87. https://doi.org/10.1038/nrmicro2666

Brangwynne, C. P., Koenderink, G. H., MacKintosh, F. C., & Weitz, D. A. (2008). Cytoplasmic diffusion: Molecular motors mix it up. *The Journal of Cell Biology*, *183*(4), 583–587. https://doi.org/10.1083/jcb.200806149

Cairns, T. C., Nai, C., & Meyer, V. (2018). How a fungus shapes biotechnology: 100 years of *Aspergillus niger* research. *Fungal Biology and Biotechnology*, *5*, 13. https://doi.org/10.1186/s40694-018-0054-5

Cairns, T. C., Zheng, X., Zheng, P., Sun, J., & Meyer, V. (2019). Moulding the mould: Understanding and reprogramming filamentous fungal growth and morphogenesis for next generation cell factories. *Biotechnology for Biofuels*, *12*, 77. https://doi.org/10.1186/s13068-019-1400-4

Cambell, C. K. (1971). Fine structure and physiology of conidial germination in *Aspergillus fumigatus*. *Transactions of the British Mycological Society*, *57*(3), 393–404.

Chen, Y. A., & Scheller, R. H. (2001). Snare-mediated membrane fusion. *Nature Reviews Molecular Cell Biology*, *2*(2), 98–106. https://doi.org/10.1038/35052017

Crank, J. (1987). Free and moving boundary problems, Oxford: Oxford University Press.

Diehl, S., Henningsson, E., Heyden, A., & Perna, S. (2014). A one-dimensional moving-boundary model for tubulin-driven axonal growth. *Journal of Theoretical Biology*, *358*, 194–207. https://doi.org/10.1016/j.jtbi.2014.06.019

Einstein, A. (1956). *Investigations on the theory of 'The Brownian Movement'*. A. D. Dover Publications, Inc. (Original work published 1926).

Elie, A., Prezel, E., Guérin, C., Denarier, E., Ramirez-Rios, S., Serre, L., … Arnal, I. (2015). Tau co-organizes dynamic microtubule and actin networks. *Scientific Reports*, *5*, 9964. https://doi.org/10.1038/srep09964

Fiddy, C., & Trinci, A. P. J. (1976). Mitosis, septation, branching and the duplicatoin cycle in *Aspergillus nidulans*. *Microbiology*, *97*(2), 169–184. https://doi.org/10.1099/00221287-97-2-169

Gougouli, M., & Koutsoumanis, K. P. (2013). Relation between germination and mycelium growth of individual fungal spores. *International Journal of Food Microbiology*, *161*(3), 231–239. https://doi.org/10.1016/j.ijfoodmicro.2012.12.006

King, R. (2015). A framework for an organelle-based mathematical modeling of hyphae. *Fungal Biology and Biotechnology*, *2*(1), 189. https://doi.org/10.1186/s40694-015-0014-2

Kirbas, C., & Quek, F. (2004). A review of vessel extraction techniques and algorithms. *ACM Computing Surveys*, *36*(2), 81–121. https://doi.org/10.1145/1031120.1031121

Kwon, M. J., Arentshorst, M., Fiedler, M., Groen, F. L. M., de Punt, P. J., Meyer, V., & Ram, A. F. J. (2014). Molecular genetic analysis of vesicular transport in *Aspergillus niger* reveals partial conservation of the molecular mechanism of exocytosis in fungi. *Microbiology*, *160*, 316–329. https://doi.org/10.1099/mic.0.074252-0

Lanzetti, L. (2007). Actin in membrane trafficking. *Current Opinion in Cell Biology*, *19*(4), 453–458. https://doi.org/10.1016/j.ceb.2007.04.017

López-Isunza, F., Larralde-Corona, C. P., & Viniegra-González, G. (1997). Mass transfer and growth kinetics in filamentous fungi. *Chemical Engineering Science*, *52*(15), 2629–2639. https://doi.org/10.1016/S0009-2509(97)00078-X

Luby-Phelps, K. (1999). Cytoarchitecture and physical properties of cytoplasm: Volume, viscosity, diffusion, intracellular surface area, *International review of cytology 1999* (Vol. 192, pp. 189–221). Academic Press. https://doi.org/10.1016/S0074-7696(08)60527-6

Meijering, E. H. W., Niessen, W. J., & Viergever, M. A. (2001). Quantitative evaluation of convolution-based methods for medical image interpolation. *Medical Image Analysis*, *5*(2), 111–126. https://doi.org/10.1016/S1361-8415(00)00040-2

Meyer, V., Fiedler, M., Nitsche, B., & King, R. (2015). The cell factory *Aspergillus* enters the big data era: Opportunities and challenges for optimising product formation. *Advances in Biochemical Engineering/Biotechnology*, *149*, 91–132. https://doi.org/10.1007/10_2014_297

Meyer, V., Punt, P. J., & Ram, A. F. J. (2010). Genetics, genetic manipulation, and approaches to strain improvement of filamentous fungi. In L. R. Lynd, H. Zhao, L. Katz, R. H. Baltz, A. T. Bull, B. Junker & A. L. Demain (Eds.), *Manual of industrial microbiology and biotechnology* (3rd ed., pp. 318–329). Washington, DC: American Society of Microbiology. https://doi.org/10.1128/9781555816827.ch22

Nanguy, S. P.-M., Perrier-Cornet, J.-M., Bensoussan, M., & Dantigny, P. (2010). Impact of water activity of diverse media on spore germination of *Aspergillus* and *Penicillium* species. *International Journal of Food Microbiology*, *142*(1-2), 273–276. https://doi.org/10.1016/j.ijfoodmicro.2010.06.031

Press, W. H. (2002). *Numerical recipes in C: The art of scientific computing* (2nd ed.). University Press.

Prosser, J. I., & Trinci, A. P. J. (1979). A model for hyphal growth and branching. *Journal of General Microbiology*, *111*(1), 153–164. https://doi.org/10.1099/00221287-111-1-153

Punt, P. J., van Biezen, N., Conesa, A., Albers, A., Mangnus, J., & van den Hondel, C. (2002). Filamentous fungi as cell factories for heterologous protein production. *Trends in Biotechnology*, *20*(5), 200–206.

Riquelme, M. (2013). Tip growth in filamentous fungi: A road trip to the apex. *Annual Review of Microbiology*, *67*, 587–609. https://doi.org/10.1146/annurev-micro-092412-155652

Rueden, C. T., Schindelin, J., Hiner, M. C., DeZonia, B. E., Walter, A. E., Arena, E. T., & Eliceiri, K. W. (2017). Imagej2: Imagej for the next generation of scientific image data. *BMC Bioinformatics*, *18*(1), 529. https://doi.org/10.1186/s12859-017-1934-z

Schindelin, J., Arganda-Carreras, I., Frise, E., Kaynig, V., Longair, M., Pietzsch, T., … Cardona, A. (2012). Fiji: An open-source platform for biological-image analysis. *Nature Methods*, *9*(7), 676–682. https://doi.org/10.1038/nmeth.2019

Schunck, T., Herrero, S., & Fischer, R. (2011). The *Aspergillus nidulans* CENP-E kinesin KipA is able to dimerize and to move processively along microtubules. *Urrent Genetics*, *57*, 335. https://doi.org/10.1007/s00294-011-0351-5

Shu, C. W. (1998). Essentially non-oscillatory and weighted essentially non-oscillatory schemes for hyperbolic conservation laws. In B. Cockburn, C.-W. Shu, C. Johnson, E. Tadmor & A. Quarteroni (Eds.), *Lecture Notes in Mathematics: Vol. 1697. Advanced numerical*

approximation of nonlinear hyperbolic equations (1697, pp. 325–432). Berlin: Springer.

Stapor, P., Weindl, D., Ballnus, B., Hug, S., Loos, C., Fiedler, A., … Hasenauer, J. (2018). PESTO: Parameter estimation toolbox. *Bioinformatics*, *34*(4), 705–707. https://doi.org/10.1093/bioinformatics/btx676

Steinberg, G. (2007). Hyphal growth: A tale of motors, lipids, and the Spitzenkörper. *Eukaryotic Cell*, *6*(3), 351–360. https://doi.org/10.1128/EC.00381-06

Steinberg, G., & Schuster, M. (2011). The dynamic fungal cell. *Fungal Biology Reviews*, *25*(1), 14–37. https://doi.org/10.1016/j.fbr.2011.01.008

Sugai-Guérios, M. H., Balmant, W., Furigo, A., Krieger, N., & Mitchell, D. A. (2015). Modeling the growth of filamentous fungi at the particle scale in solid-state fermentation systems. *Advances in Biochemical Engineering/Biotechnology*, *149*, 171–221. https://doi.org/10.1007/10\textunderscore

Trinci, A. P. J. (1971). Exponential growth of the germ tubes of fungal spores. *Journal of General Microbiology*, *67*(3), 345–348. https://doi.org/10.1099/00221287-67-3-345

Trinci, A. P. J. (1974). A study of the kinetics of hyphal extension and branch initiation of fungal mycelia. *Journal of General Microbiology*, *81*(1), 225–236. https://doi.org/10.1099/00221287-81-1-225

Virag, A., & Harris, S. D. (2006). The Spitzenkörper: A molecular perspective. *Mycological Research*, *110*(1), 4–13. https://doi.org/10.1016/j.mycres.2005.09.005

Yang, H., King, R., Reichl, U., & Gilles, E. D. (1992). Mathematical model for apical growth, septation, and branching of mycelial microorganisms. *Biotechnology and Bioengineering*, *39*(1), 49–58. https://doi.org/10.1002/bit.260390109

SUPPORTING INFORMATION

Additional supporting information may be found online in the Supporting Information section.

How to cite this article: Kunz PJ, Barthel L, Meyer V, King R. Vesicle transport and growth dynamics in *Aspergillus niger*: Microscale modeling of secretory vesicle flow and centerline extraction from confocal fluorescent data. *Biotechnology and Bioengineering*. 2020;117:2875–2886. https://doi.org/10.1002/bit.27452